ELSEVIER

International Journal of Mass Spectrometry 220 (2002) 289–312

International Journal of Mass Spectrometry

www.elsevier.com/locate/ijms

Vibrational spectroscopic evidence of unconventional hydrogen bonds

Asuka Fujii, G. Naresh Patwari, Takayuki Ebata, Naohiko Mikami*

Department of Chemistry, Graduate School of Science, Tohoku University, Aoba-ku, Sendai 980-8578, Japan

Received 10 December 2001; accepted 11 February 2002

Abstract

In this article, infrared (IR) spectroscopic evidence for two classes of unconventional hydrogen bonds is presented. The first one involves drastic change in the hydrogen bonding properties in cationic states relative to neutral species. The phenol–benzene cluster shows an extremely high enhancement of π-hydrogen bonding interaction upon ionization. On the other hand, the benzene–water cluster shows a dramatic change from the π-hydrogen bonded to C–H···O type hydrogen bonded structure following ionization. In the case of alkyl phenols, the O–H stretching vibration of *o–cis*-isomer is shifted to a lower frequency upon ionization, which reflects the formation of an unconventional hydrogen bond of the type O–H···C, wherein the alkyl carbon acts as a proton acceptor. The second is novel hydrogen bonding between borane–amines and acidic protons. The vibrational spectra of O–H and N–H stretching vibrations in phenol and 2-pyridone (2PY), respectively, clearly indicate that these compounds act as proton donors to borane–amines. The experimental observations along with the density functional theoretical (DFT) calculation clearly establishes the formation of "dihydrogen bonding" between the O–H/N–H and B–H groups. Further, the two interacting hydrogens in a dihydrogen bond get eliminated as molecular hydrogen in the cluster cation leading to dehydrogenation reaction. (Int J Mass Spectrom 220 (2002) 289–312)

Keywords: Hydrogen bond; Infrared; Vibrational spectroscopy

1. Introduction

The concept of hydrogen bonding is central to chemistry and biology [1–3]. The role of hydrogen bonding has been well established in characterization of, properties of water, crystal structures of ice, gas hydrates, self-assembling systems, stabilization of biological macromolecules, selective binding of substrates to biological macromolecules, as a precursor to proton transfer reactions and in a variety of other systems. Historically, many experimental techniques, such as, heats of formation, X-ray crystallography, electron diffraction analyses, infrared (IR)/Raman, microwave, and NMR spectroscopic techniques along with theoretical analyses have been employed to investigate the nature of hydrogen bonding. Apart from the conventional phases of matter, hydrogen bonding has been investigated in a wide range of environments, from weakly interacting systems, such as noble gas matrices, to strongly interacting systems, such as living cells. The developments in various experimental as well as theoretical techniques, over the years, used for investigation of hydrogen

* Corresponding author.
E-mail: nmikami@qclhp.chem.tohoku.ac.jp

1387-3806/02/$ – see front matter
PII S1387-3806(02)00774-1

bonded systems has greatly enhanced our understanding of their structure and dynamics at a microscopic level.

Over the last two decades, the combination of laser spectroscopy and molecular beam techniques has seen the emergence of a new field called cluster chemistry [4]. This new field of chemistry contributes in our effort to achieve more insights on intermolecular interactions at an unprecedented microscopic level. The versatile supersonic jets and beams technique can be used to produce clusters, which are molecular entities bound by weak intermolecular interactions, such as van der Waals forces or hydrogen bonding, by co-expansion of required reagents. Molecular clusters produced under cold and isolated condition of supersonic jets allows us to probe structures, intermolecular potentials, and dynamics at microscopic level with the aid of various laser spectroscopic techniques.

Most of the earlier works on the hydrogen bonded clusters in molecular beams were carried out using electronic spectroscopy [5]. Electronic spectra of clusters exhibit characteristic spectral shifts depending on their size and/or structural differences. However, the relation between the shifts and the nature of hydrogen bonding is often not straightforward. More seriously, electronic spectra frequently show spectral congestion and/or poor Franck–Condon factors for the transitions involving high frequency vibrations, such as hydride stretching, which are directly involved in the hydrogen bonding and carry the key information. In order to obtain more precise information about hydrogen bonds it is imperative to carry out vibrational spectroscopy of clusters in molecular beams.

Vibrational spectroscopy of protic groups, such as O–H, N–H, and sometimes C–H, has long been realized as the most important spectroscopic tool to identify hydrogen bonding [1,2]. This is due to the fact that these vibrations are very sensitive to hydrogen bonded structures, and show characteristic frequency shifts upon hydrogen bonding. However, vibrational spectroscopy of the clusters in supersonic beams cannot be achieved with conventional absorption measurements, even by using an advanced FTIR spectrometer. The difficulties arise due to very low density of a desired cluster in a heavy mixture of other clusters and monomers/bare molecules. In this respect, any spectroscopic technique to be used for the investigation hydrogen bonded clusters requires merits of having high sensitivity and selectivity.

Lee and co-workers first demonstrated the IR spectroscopy of clusters by population labeling of target species using electronic transition, which enables the size/structure selection [6]. Brutschy and co-workers applied this technique to hydrogen bonded clusters for the first time to fluorobenzene–methanol clusters, wherein they observed the C–O stretching vibration of methanol [7]. In this case, due to the restriction in laser source the technique was limited to C–O stretching. Hydrogen bonded O–H stretching vibrations of well defined clusters were first observed by Mikami and co-workers and by Pribble and Zwier simultaneously in phenol–water and benzene–water clusters, respectively [8,9]. In combination with quantum chemical calculations, such as ab initio molecular orbital or density functional methods, these studies establish unequivocally intermolecular structures and binding energies of size-selected clusters in jet-cooled molecular beams [10–12].

The majority of hydrogen bonding observed, both in chemistry and biology, is the interaction between an acidic proton, such as O–H or N–H groups, and a lone pair of electrons on an electronegative element such as O or N or halogen (referred as conventional/σ-hydrogen bond here onwards). Though, comparatively less, reasonable numbers of reports exist in the literature wherein the hydrogen bonding is between an acidic proton and π-bond electrons [1–3,13,14]. Crystallographic and ab initio quantum chemical calculations, over the last decade, have also established the proton donating ability of a methyl group and formation of a weak hydrogen bonding of the type C–H$\cdots$X (X = N, O) bonds [2,3,15–19]. This weak inter-/intramolecular hydrogen bonding involving methyl/methylene groups is believed to play an important role in protein folding, carbohydrate structure and many other processes

involving biological macromolecules. Investigations on such a weak interaction involving methyl/methylene groups and comparison between the neutral and ionic manifolds will provide us with insights, which can enhance our understanding of higher order structures of biological macromolecules. Experimentally, however, it is extremely difficult to investigate the role of cationic character on this weak hydrogen bonding in condensed phases or in matrices, because of a substantial perturbation from the environment. In sharp contrast, the spectroscopy of size-selected clusters in supersonic molecular beams has opened up the possibility of investigating the unconventional hydrogen bonds involving C–H groups and their dependence on cationic character. For experimentalists the perturbation free environment provided by molecular beams presents a unique challenging opportunity to investigate and identify interactions, which are not always possible in condensed phases.

In this article, we will focus on two cases of unconventional hydrogen bond. The first one is the enhancement of hydrogen bonding interaction in cationic states. In condensed phases, especially in solution, cations of molecules or clusters polarize their environment extensively leading to dominant electrostatic interactions, which often mask weaker interactions present in the cations. On the other hand, molecular cations prepared in a jet-cooled molecular beam are free from perturbations originating from environment, and are suitable for investigating weak interactions. We have found unambiguous evidence of a through-space interaction between an O–H group and a methyl group in *o*-methylphenol (cresol) cation [20,21]. This through-space interaction in the ionic manifold can be called hydrogen bond, since its spectroscopic characteristics are identical to those of a conventional hydrogen bond. Further, we found substantial enhancement of π-hydrogen bonding in cationic systems, which is sometimes accompanied by a large structural change induced by ionization [22,23].

The second class of unconventional hydrogen bonded systems involves a new type of hydrogen bond acceptors. It has been found in the crystals of several borane–amines that the B–H σ-bond acts as a proton acceptor for the N–H group, leading to the formation of an unconventional hydrogen bond of the type B–H···H–N [24]. A similar unconventional hydrogen bond was also observed in outer coordination sphere of several transition metal complexes, wherein metal–hydrogen σ-bonds (M–H) act as proton acceptors to an acidic N–H/O–H group [24,25]. This interaction between boron/metal hydride and acidic proton can be generically represented as E–H···H–X, wherein E and X are electropositive and electronegative atoms, respectively, with respect to hydrogen, and was termed as “dihydrogen bond” [26]. Structurally, the crystallographic data show that the contact distance between the two interacting hydrogens is less than 2.2 Å and also show a remarkable statistics of a strongly bent B–H···H angle averaging around 100° [24], whose origin is not yet understood. Despite the large set of crystallographic data, structural studies on “dihydrogen bond” in crystals are not adequate to investigate its inherent nature, because the bond may largely be perturbed by ligand fields and packing forces. The intrinsic characteristics of the dihydrogen bond should be investigated in an environment free condition such as a jet-cooled molecular beam. Another important aspect of dihydrogen bonding is the elimination of two interacting hydrogens as molecular hydrogen, leading to dehydrogenation reaction [27,28]. This reaction is thermodynamically favorable due to a large free energy for the formation of H_2. We look at the formation of dihydrogen bonded clusters between proton donors, such as phenol [29,30] and 2-pyridone (2PY) [31], and borane–amine adducts and also the dehydrogenation reaction via dihydrogen bonding in the gas phase [27].

The presentation of this paper is as follows; a brief description of various experimental techniques used for the characterization of unconventional hydrogen bonded systems in molecular beams is given in the next section. The hydrogen bonding in cations is presented in Section 3 and results on dihydrogen bonded systems are discussed in Section 4. The concluding remarks are presented in the final section.

2. Experimental

A variety of experimental techniques have been used for complete spectroscopic identification and characterization of bare molecules and molecular clusters in supersonic jets [10–12]. As mentioned in the previous section the much-required selectivity of the neutral clusters is provided by electronic transitions, which can be monitored using either fluorescence and/or resonance enhanced multiphoton ionization (REMPI) induced by an ultraviolet (UV) laser. The combined technique is called IR–UV double resonance spectroscopy [6,8], and has been applied to various neutral clusters, as along as they show a distinct sharp transition in their $S_1 \leftarrow S_0$ electronic spectrum. The identification of particular species among cluster of various sizes and structures (isomers) can be done using mass spectrometry with REMPI along with IR–UV [32] or UV–UV [33] hole-burning spectroscopy.

Vibrational excitation of cluster cations due to IR absorption is followed by vibrational predissociation, resulting in the production of fragment ions. By monitoring the fragment ions, highly sensitive detection of the IR absorption can be performed. This method is called infrared photodissociation (IRPD) spectroscopy [34–38]. In the case of bare molecular cations, however, such IR photodissociation is not expected because of much higher dissociation energies for the covalent bonds compared to intermolecular bonds. Further, IR–UV spectroscopy is also not adequate because electronic transitions of molecular cations are mostly broad, especially in the case of aromatics. Therefore, we proposed a new IR spectroscopic technique called autoionization detected infrared (ADIR) spectroscopy [39,40], in which high Rydberg states are utilized as a probe of IR absorption of the ion core, which is essentially the same as the molecular cation. At present, this technique (and its variation [41]) is unique IR spectroscopy applicable to jet-cooled bare aromatic cations. Below, we give a brief description of various techniques used.

2.1. IR–UV double resonance spectroscopy for the neutral ground state

A pulsed UV laser whose wavelength is fixed at the origin band of the $S_1 \leftarrow S_0$ transition of a target species is introduced, and the S_1 fluorescence or REMPI signal is monitored as a measure of the ground state population. Prior to the UV laser, an IR laser is introduced, and its wavelength is scanned. When the IR wavelength is resonant with a vibrational transition of the species, the IR absorption induces reduction of the population, which is then detected as a decrease in the fluorescence or REMPI signal intensity. The resultant spectrum is called fluorescence detected IR (FDIR) or ion detected IR (IDIR) spectrum depending upon the detection scheme used.

2.2. Hole-burning spectroscopy

Two versions of hole-burning spectroscopy have been used in order to distinguish sizes and isomers of clusters. The first one is the UV–UV hole-burning spectroscopy, wherein a tunable intense UV pulse pumps the ground state molecules to the excited state. Another weak UV pulse, whose wavelength is tuned to a vibronic band of a specific cluster, arriving after an appropriate delay-time probes the population of the cluster. The fluorescence (or ion signal) due to the probe laser is monitored as a function of the pump laser wavelength. In the situation, when the pump laser wavelength is resonant with the vibronic transition of the cluster that is being probed, it depletes the ground state population, and the fluorescence due to the probe laser shows a dip, thereby providing the origin of that particular transition.

The second version is IR–UV hole-burning spectroscopy. In this spectroscopy, a $S_1 \leftarrow S_0$ electronic spectrum is recorded for the region of interest. Following, an IR pulse is tuned to a vibrational transition of a specific cluster while a delayed tunable UV laser probes the $S_1 \leftarrow S_0$ transition region. In the event of the UV laser being resonant with the transition of the same cluster to which the IR pulse is tuned to, the

intensity of fluorescence decreases when compared to the first spectrum. Subtraction of the second spectrum from the first one allows identifying the relevant transitions.

2.3. Autoionization detected infrared spectroscopy for molecular cations

Two-color double resonance excitation is used to pump a molecule to its high Rydberg state(s) lying just below the first ionization threshold (IP_0). When the ion core of the Rydberg states is vibrationally excited by an IR light pulse, the total energy of the Rydberg states exceeds IP_0 because of the vibrational energy of the ion core. Then, vibrational autoionization (the energy transfer process from the vibration of the ion core to the Rydberg electron) takes place, resulting in the generation of the molecular ions. Thus, the IR spectrum is obtained by monitoring the ion intensity as a function of the IR wavelength. Observed vibrational frequencies are practically regarded as being identical to those of the bare ion because of the extremely weak interaction between the ion core and the high Rydberg electron.

2.4. Infrared photodissociation spectroscopy for cluster cations

Bare molecules are photoionized with REMPI in the expansion region of the pulsed jet, so that the cluster cations are efficiently formed by collisions with other molecules. The produced cluster cations are lead into a radio frequency ion trap cell of the Paul type, and are trapped. Then, an IR light pulse is introduced into the trapped region of the cell, and its wavelength is scanned. When the IR wavelength is resonant on vibrational transitions of the cluster ion, the vibrational excitation followed by IR multiphoton absorption causes vibrational predissociation of the parent cluster ion, leading to the production of fragment cations. After the IR irradiation, all the cations are ejected from the cell by applying a pulsed electric field, and the fragment ions are mass analyzed with a mass filter. Thus, by scanning the IR wavelength while monitoring the fragment cation intensity, the IR spectrum of the parent cluster ion is obtained.

3. Hydrogen bonding in cations

3.1. Photoionization of π-hydrogen bonded clusters

3.1.1. Enhancement of π-hydrogen bond; phenol–benzene

It is well known that π-electrons in a multiple bond act as proton acceptors, and this type of interaction is called a π-hydrogen bond [1–3,13,14]. In the neutral manifold, the typical strength of π-hydrogen bonds is considerably weaker ($\leq$5 kcal/mol) than that of σ-hydrogen bonds ($\approx$10 kcal/mol). It has been found that, following ionization of σ-hydrogen bonded cluster, the proton donating ability of a donor site enhances considerably, leading to a substantial enhancement of the hydrogen bond in the cation [42]. In contrast, π-hydrogen bonds in cationic states have not yet been well characterized. In some cases, the hydrogen bonded interaction of a π-hydrogen bond in the cationic state is expected to exceed over that of a σ-hydrogen bond in the neutral cluster. The phenol–benzene binary cluster presents a typical example of such a behavior of the extreme enhancement of π-hydrogen bond strength upon ionization.

Fig. 1 shows the IDIR spectra in the O–H stretching of (a) bare phenol and (b) phenol–benzene in the neutral ground state. In the case of bare phenol the O–H stretching vibration can be seen at 3657 cm^{-1} [8,43], while that of the phenol–benzene cluster appears at 3579 cm^{-1}. These results are in good agreement with the earlier reported values, using ionization detected Raman spectroscopy [44]. The O–H stretching vibration of the cluster shows a shift of 78 cm^{-1} to a lower frequency. This shift in phenol–benzene is substantially smaller than those found in typical σ-hydrogen bonded clusters of phenol with proton acceptors, such as water ($-133\,cm^{-1}$), methanol ($-201\,cm^{-1}$), ammonia ($-363\,cm^{-1}$), and trimethylamine ($-590\,cm^{-1}$), in which the phenolic O–H is bound to the lone pair of the acceptor [45]. The small

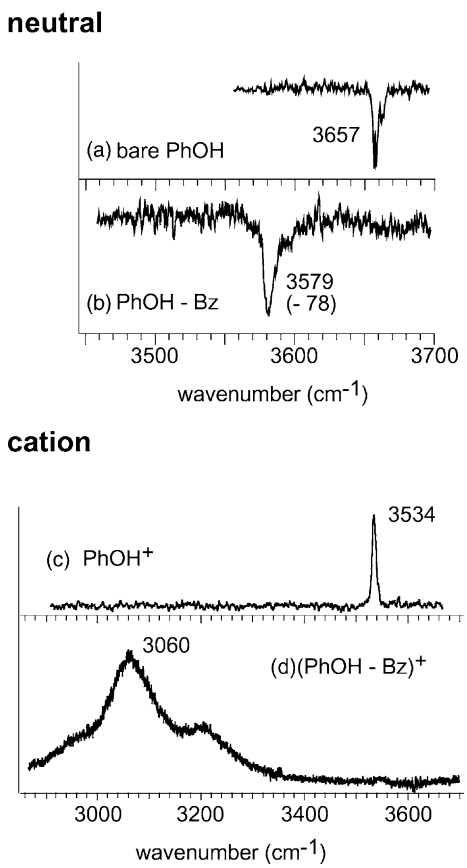

Fig. 1. (Upper panel) The O–H stretching vibrational region of IR spectra of (a) bare phenol (PhOH) and (b) phenol–benzene (PhOH–Bz) cluster in the neutral ground state. The IDIR spectroscopy is used to measure the spectra. (Lower panel) The 3 μm region of IR spectra of (c) bare $PhOH^+$ cation and (d) $(PhOH–Bz)^+$ cation obtained by ADIR and IRPD spectroscopy, respectively.

shift in the present case clearly indicates that the phenol moiety is bound by a π-hydrogen bond to the benzene moiety, whose aromatic ring is the unique proton accepting site.

The IR spectra of the bare phenol cation and the $(phenol–benzene)^+$ cluster cation in the 3 μm region are shown in Fig. 1(c) and (d), respectively. The ADIR and IRPD techniques were utilized to observe the IR spectra of the bare molecular cation and the cluster cation, respectively. The O–H stretching of the bare cation can be seen at 3534 cm^{-1}, which shows a shift of 123 cm^{-1} to a lower frequency upon ionization [39,40]. This shift is believed to be due to an enhancement of the double bond character of the C–O bond and the resulting reduction of the O–H force field. In the case of the cluster cation, the IR spectrum shows an intense and broad band at 3060 cm^{-1} with no band above 3300 cm^{-1}. The IR spectrum of the phenol–benzene deuterated cluster cation, $(C_6D_5OH–C_6D_6)^+$, which was measured by Inokuchi and Nishi [46], has the same spectral feature. Therefore, the band at 3060 cm^{-1} was uniquely assigned to the O–H stretching vibration of the cluster cation, which shows an extremely large shift of over 470 cm^{-1} to a lower frequency. Because of the large difference in the ionization potentials between phenol (68,625 cm^{-1}) [47] and benzene (74,556 cm^{-1}) [48], the positive charge is mostly localized on the phenol moiety in the cluster cation. Therefore, the π-hydrogen bond must be preserved even in the phenol–benzene cluster cation. Though the hydrogen bond in the cation is of the π-type, the O–H shift is quite large (over 470 cm^{-1}), and is six times larger than that of the neutral cluster. Moreover, this shift is as large as those in the neutral phenol–ammonia and phenol–trimethylamine σ-hydrogen bonded clusters [45]. If we simply assume a linear correlation between the hydrogen bond strength and the shifting of O–H stretching vibration to a lower frequency, this result suggests that the π-hydrogen bond in the cluster cation is as strong as the conventional hydrogen bonds with strong base molecules in their neutral manifold. Because of the enhancement of the acidity of the donor moiety and electrostatic and induction interactions, the π-hydrogen bond in the cluster cation is no longer a weak hydrogen bond.

In the IR spectrum of phenol–benzene cluster cation (Fig. 1(d)) a weak and broad shoulder band can be seen around 3220 cm^{-1}. Similar shoulder structures associated with the π-hydrogen bonded O–H stretching vibration were also observed for phenol–ethylene and phenol–acetylene cluster cations [49]. The frequency difference between the O–H stretching band and the shoulder band in all the three cases is almost constant (150–170 cm^{-1}), and also the relative intensities are quite similar. The constant frequency difference

between the O–H stretching band and the shoulder band in spite of the large mass difference among the proton acceptors, viz. benzene, ethylene, and acetylene, rules out the possibility of intermolecular vibration in combination with O–H stretching vibration. Therefore, this shoulder band is assigned to the O–H bending overtone band borrowing the intensity from the neighboring O–H stretching vibration. This assignment is also supported by similar appearance of O–H bending overtone bands in hydrated anion clusters, in which hydrogen bonded O–H stretching vibrations are shifted to down to 3000–3200 cm^{-1} region [50].

Though it is difficult to exactly estimate the strength of π-hydrogen bond in the phenol–benzene cluster cation, its lower limit can roughly be estimated by considering the charge resonance (CR) interaction for the cationic state. If the phenol–benzene cluster cation exhibits a sandwich-type form consisting of a parallel conformation of a pair of the aromatic rings, similar to the benzene dimer cation, the binding energy of the cluster cation will be given by the CR interaction [51]. The energy due to the CR interaction (ΔE_{CR}) is given by

$$\Delta E_{CR} = -\frac{\Delta IP}{2} + \frac{1}{2}\{(\Delta IP)^2 + 4\varepsilon^2\}^{1/2}$$

where ΔIP is the difference of the ionization potentials between two components of the dimer and ε is the CR interaction matrix element. For phenol and benzene, ΔIP is 0.735 eV, and ε is assumed to be 0.67 eV, which is the same value as the benzene dimer cation [52,53]. Then, the ΔE_{CR} is roughly estimated to be 0.4 eV (≈9 kcal/mol). Because the CR interaction prefers the parallel sandwich form as seen in the benzene dimer cation, it is not applicable for the π-hydrogen bond, which has a non-parallel conformation of the two aromatic rings. When the CR interaction is effective, a characteristic transition, called a CR band, should appear in the near IR region [52]. The phenol–benzene cluster cation, however, has no strong absorption in this region, supporting the non-parallel structure due to the π-hydrogen bond [51]. This result indicates that the π-hydrogen bonding energy in the cation is dominant over the CR interaction. It is, therefore, concluded that the π-hydrogen bond strength in the cation (phenol–benzene)$^+$, is larger than the CR stabilization energy, 0.4 eV (≈9 kcal/mol).

Thus, the estimated π-hydrogen bond strength in the phenol–benzene cation is found to be much larger than binding energies in its neutral state and even in σ-hydrogen bonded neutral clusters. Though binding energies of π-hydrogen bonded clusters have not been precisely determined experimentally, the upper limit of the binding energy of phenol–benzene in S_0 was estimated to be in the range of 0.155–0.192 eV in the time-resolved photo-fragment detection study reported by Knee et al. [54]. The binding energies have also not been determined experimentally for any σ-hydrogen bonded clusters of phenol. Because the acidity of 1-naphthol (pK_a = 9.34) is very similar to that of phenol (pK_a = 9.89) [55], the hydrogen bonded clusters of phenol are expected to have a similar binding energy as those of 1-naphthol. The binding energies for the σ-hydrogen bonded 1-naphthol clusters with methanol and with ammonia in S_0 were determined to be 0.328, and 0.332 eV, respectively, by using the stimulated emission pumping spectroscopy [56].

3.1.2. Disappearance of π-hydrogen bond; benzene–H_2O

As described above, photoionization of the phenol–benzene cluster localizes the positive charge on the donor (phenol) site leading to a remarkable enhancement of the π-hydrogen bond strength. On the other hand, when the charge is created on the acceptor site, the situation is expected to be quite different from the phenol–benzene case. A typical example is the π-hydrogen bonded benzene–water cluster, wherein the aromatic ring is acting as a hydrogen bond acceptor to water in the neutral state. Upon ionization the positive charge is expected to localize on the accepting (benzene) site, because of a large difference in ionization potential between benzene and water. As a result, the proton donor (water) is expected to be repelled from the ring, which may lead to a large change in the π-hydrogen bond structure.

The benzene–water cluster has been the most extensively studied π-hydrogen bonded cluster [57–64]. Microwave and IR spectroscopic studies of this cluster have demonstrated that the water molecule is symmetrically π-hydrogen bonded on the center of the benzene ring in S_0. Several theoretical calculations, on the other hand, have predicted the disappearance of the π-hydrogen bond accompanied by extensive structural changes upon ionization [65–67]. Both ab initio and density functional theoretical (DFT) calculations have demonstrated the absence of a minimum in the potential corresponding to the π-hydrogen bonded form of $(Bz–H_2O)^+$ [65–68]. The most stable structure for $(Bz–H_2O)^+$ is shown as an inset in Fig. 2, in which two hydrogen atoms of the benzene interact with the oxygen atom of water forming a pair of the C–H···O hydrogen bonds. The charge–dipole interaction is a major component of the intermolecular bond in this structure.

Fig. 2(a) shows the IRPD spectra of $(Bz–H_2O)^+$ in the C–H and O–H stretching region. Three bands seen at 3720, 3635 and 3090 cm^{-1} were assigned to the anti-symmetric (ν_3) and the symmetric O–H stretching vibration (ν_1) of the water site, and the C–H stretching vibrations of the benzene cation site, respectively. A similar spectrum of $(Bz–H_2O)^+$ in the O–H stretching region was also reported by Solcà and Dopfer [68]. A remarkable enhancement of the absorption intensity of the ν_1 band was observed relative to the ν_3 band. This phenomenon is usually observed in hydrated cluster cations [34–38]. In the case of the neutral $Bz–H_2O$ cluster, the O–H stretching bands of the water site exhibit complicated features attributed to the coupling with free rotation of the water molecule around the C_6 axis of the benzene ring [59]. In the cation spectra, no such feature is seen for the O–H band, indicating that the rotation of the water molecule in $(Bz–H_2O)^+$ is frozen.

Another remarkable feature of the IR spectrum of $(Bz–H_2O)^+$ is that the intensity of the C–H stretching band is as strong as the O–H stretching bands, in spite of the fact that the intensity of the aromatic C–H stretching in molecular cations is generally much weaker than those of O–H stretches [39,40,69,70].

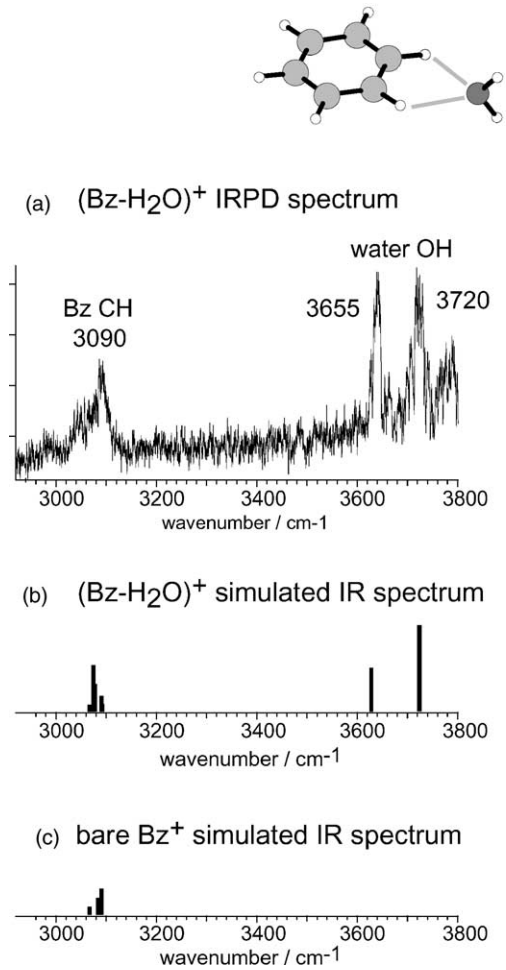

Fig. 2. (a) IRPD spectrum of $(Bz–H_2O)^+$ in the 3 μm region. (b) Simulated IR spectrum of $(Bz–H_2O)^+$ based on the energy optimized structure. (c) Simulated IR spectrum of bare Bz^+. The intensities of the simulated spectra are plotted in the common scale. Inset is the energy optimized structure of $(Bz–H_2O)^+$ at the B3LYP/6-31G (d,p) level of calculations.

This appears in a sharp contrast to the neutral $Bz–H_2O$ cluster, in which the water molecule on the benzene ring does not perturb the C–H stretching vibrations [58]. The remarkable enhancement of the C–H stretching intensity indicates a substantial perturbation of the C–H groups of benzene by the water molecule in the cluster cation.

The simulated IR spectrum for $(Bz–H_2O)^+$ is shown in Fig. 2(b), corresponding to the energy optimized

structure of the side bound form, shown in the inset of Fig. 2. Also shown is the simulated spectrum of the bare benzene cation in Fig. 2(c) for comparison. The observed band positions and intensities of both the O–H and C–H stretching vibrations are well reproduced in the simulated spectrum. The excellent agreement between the observed and simulated spectra clearly indicates that the cluster cation has the side bound structure. Furthermore, the intensities of the C–H stretching vibrations of the cluster cation are significantly enhanced relative to those of the bare benzene cation, and are as strong as O–H stretching vibrations. The enhancement must be due to the formation of the C–H···O hydrogen bonding, which leads to the creation of a permanent dipole moment on the aromatic ring.

3.2. New type of intramolecular hydrogen bond

Hydrogen bonds involving alkyl groups have been controversial in chemistry [1–3]. Crystallographic and theoretical studies suggest the formation of a very weak C–H···X hydrogen bond [13,15–19]. Moreover, most of the studies on such an interaction of alkyl groups, so far, are concerned with those in their neutral ground state. As shown in the above sections, recent spectroscopic studies on hydrogen bonded cluster cations have shown that the hydrogen bond strength drastically changes upon ionization. This suggests that the hydrogen bonds involving alkyl groups in the cationic state would also be very different from that in the neutral state. In this respect, alkyl-substituted phenol cations are expected to be an appropriate system for a spectroscopic investigation of weak hydroxyl–alkyl interactions.

Cresol (methylphenol), for example, has many rotational and structural isomers with respect to the conformation and/or substitution position of the hydroxyl group relative to the alkyl group [71–74], exhibiting a large variation of the alkyl–hydroxyl interactions. Since the O–H stretching vibration is a very sensitive probe of the hydrogen bonding strength, a comparison of the O–H stretching frequencies among the structural and rotational isomers both in the neutral and cationic states is expected to provide direct information on the alkyl–hydroxyl interactions. Fig. 3 shows IDIR spectra of various rotational and structural isomers of jet-cooled neutral cresol. These spectra were recorded by probing the REMPI signal via the $S_1 \leftarrow S_0$ transition, which are different for each isomer [71–74]. Sharp dips in all the spectra correspond to the O–H stretching vibrations, all of which are within 3 cm^{-1} and are very close to that of bare phenol (3657 cm^{-1}). This suggests that the methyl substitution causes a negligible perturbation on the force field in the hydroxyl group. In the *cis*-isomer of *o*-cresol, intramolecular hydrogen bond formation is expected between the neighboring hydroxyl and methyl groups. On the other hand, it is clear that such an intramolecular hydrogen bond is not possible in the *trans*-isomer because of a steric restriction. The *cis*- and *trans*-isomers of neutral *o*-cresol show essentially the same O–H frequency, indicating that the intramolecular hydrogen bond, if any, is negligible in neutral *o*-cresol.

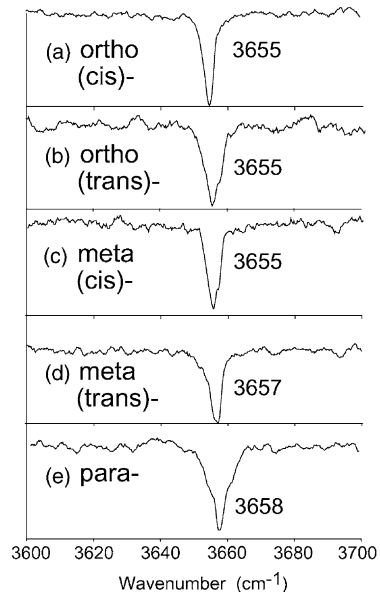

Fig. 3. IDIR spectra of isomer-separated neutral cresol in the O–H stretching vibrational region.

ADIR spectra of the O–H stretching vibrations of cresol cations are shown in Fig. 4. Unlike the neutral cresols the O–H stretching vibration in the

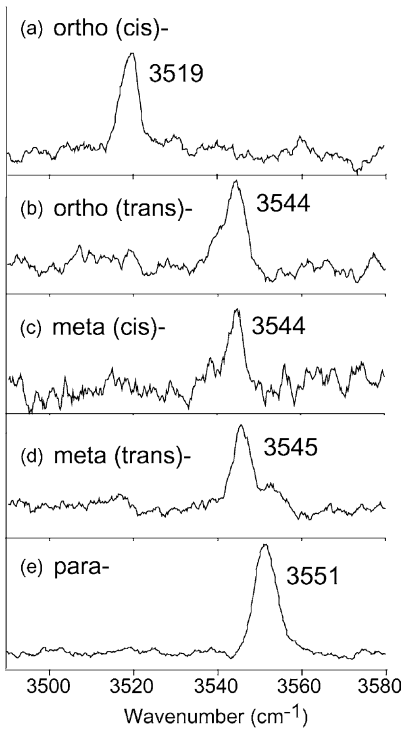

Fig. 4. ADIR spectra of isomer-separated cresol cations in the O–H stretching vibrational region.

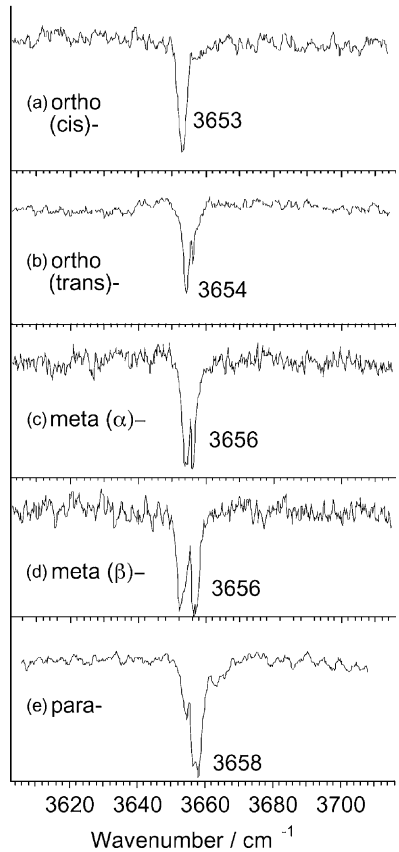

Fig. 5. IR spectra of isomer-separated neutral ethylphenol in the O–H stretching vibrational region. The notations of the *m*-isomers are taken from [21].

o–*cis*-isomer (3519 cm^{-1}) shows a substantially larger shift to a lower frequency in comparison with all the other isomers (≈3545 cm^{-1}), which is rather remarkable. If this is due to the electronic interaction between O–H and CH_3 groups through the phenyl ring, the *trans*-isomer of the *o*-cresol cation should exhibit the same (or at least similar) shift as the *cis*-isomer. The observed result, however, shows the O–H frequency of *o*–*trans*-isomer is almost same as in *m*- and *p*-isomers. Therefore, the origin of this characteristic shift for the *cis*-isomer of the *o*-cresol cation is due to local interactions between O–H and CH_3 groups, i.e., intramolecular hydrogen bonding. The configuration of the *cis*-isomer and the shifting of O–H stretching vibration to a lower frequency indicate that the methyl group should be the proton acceptor for the hydroxyl group. Such an unconventional interaction has never been reported and this is the first observation of a new type of intramolecular hydrogen bond.

Further spectroscopic evidence for the unconventional intramolecular hydrogen bonding can be found in ethylphenol cations. Fig. 5 shows IDIR spectra in the O–H stretching region of *o*-, *m*-, and *p*-ethylphenol in the neutral ground state. All the O–H stretching frequencies, including that of the *o*–*cis*-isomer, are very close to that of free phenol (3657 cm^{-1}), indicating that the ethyl substitution causes a negligible perturbation on the force field of the O–H bond stretching. The observed splitting of O–H stretching band is due to IR absorption of ambient water vapor, which modulates the IR power. ADIR spectra in the O–H stretching region of *o*- and *p*-ethylphenol cations are shown in Fig. 6. The *cis*-isomer of the *o*-ethylphenol

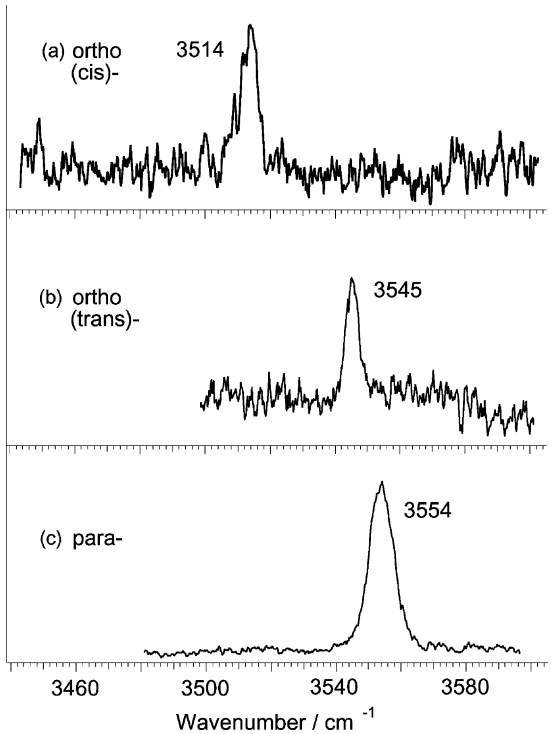

Fig. 6. ADIR spectra of isomer-separated ethylphenol cations in the O–H stretching vibrational region.

cation shows a substantial lower O–H stretching frequency (3514 cm^{-1}) compared to the *trans*-isomer (3545 cm^{-1}) and *p*-ethylphenol cation (3554 cm^{-1}). This phenomenon is quite similar to that observed in the *o*-cresol cation.

The difference in O–H stretching frequency between the *cis*- and *trans*-isomer cations of *o*-cresol and *o*-ethylphenol are 25 and 31 cm^{-1}, respectively. From these two similar observations, therefore, it is reasonable to conclude that the remarkable shift of the O–H stretching vibration to a lower frequency in the *cis*-isomer cation is due to the intramolecular hydrogen bonding with the neighboring alkyl group, which acts as a proton acceptor. Furthermore, these shifts are comparable to the those observed due to intramolecular hydrogen bond in neutral *o*-fluorophenol, suggesting the same order of the hydrogen bond strength [40]. A very weak O–H···C type intermolecular hydrogen bond was predicted by ab initio calculations of the CH_4–H_2O cluster [75] with extremely small binding energy of 0.83 kcal/mol. This is consistent with undetectable lowering of the O–H stretching vibration in neutral *cis*-isomer of *o*-cresol.

At present, it is difficult to provide an unequivocal explanation for the appearance of hydrogen bonding upon ionization. The O–H frequency shift associated with the intramolecular hydrogen bonding is very small, and requires an extremely careful theoretical examination, particularly for ionic states. Though we calculated the structure of the *o*-cresol cations by using Hartree–Fock and DFT calculations (B3LYP) with 6-31G (d,p) basis set, which usually are very effective for analysis of conventional hydrogen bonding systems [10], we failed to reproduce the observed difference in the O–H stretching frequency between the *cis*- and *trans*-isomer cations. Recently, MP2/6-31G (d) and B3LYP/6-311+G (d,p) calculations on the *o*-cresol cations were reported by Trindle [76], and also HF/6-31+G (d,p) and B3LYP/6-31+G (d,p) level calculations were carried out by Vank et al. [77]. Though both the groups gave negative conclusions on the presence of the new type of the intramoleular hydrogen bond based on these calculations, their calculations did also not reproduce the experimental results; they seriously underestimated difference in the O–H stretching frequency between the *cis*- and *trans*-isomers of the *o*-cresol cations. To capture implications of such small but significant O–H stretching frequency shifts, much higher-level calculations are clearly required.

In the case of alkylphenols the charge is delocalized not only in the phenyl ring but also on the alkyl and hydroxyl groups. Presently, we are considering the possibility of a carbo-cation mechanism. The partially positive-charged carbon of CH_3 (CH_2) group in the cation can be considered as a five coordinate site associated with the three-center two-electron bond. The presence of this type of non-classical cations, such as CH_5^+, has been confirmed [78]. The methyl group in cresol is positively charged because of its electron donating ability to the phenyl ring, and the partial charge increases upon ionization. Such an increase

of the charge distribution might induce the mixing of such non-classical character, which contributes to the intramolecular hydrogen bond.

4. Dihydrogen bonding and dehydrogenation reaction

4.1. Dihydrogen bonded clusters

4.1.1. Phenol–BTMA

It is known from numerous crystal structures of borane–amine adducts reported in the Cambridge Crystallographic Database that a B–H bond in borane–amine acts as a proton acceptor for the N–H group leading to the formation of dihydrogen bond [24]. On the other hand, various clusters of phenol with water, alcohols, and amines, investigated in our laboratory using electronic and vibrational spectroscopy, have established the proton donating ability of phenol [45]. Therefore, one can deduce, straightforwardly, that borane–amines form a dihydrogen bond with phenol. Experimentally, this was achieved by the co-expansion of phenol and borane-trimethylamine (BTMA) vapor seeded in helium buffer gas to form a supersonic jet. The LIF excitation spectrum of the resultant mixture around the $S_1 \leftarrow S_0$ band origin transition of phenol is shown in Fig. 7(a). Many transitions in this spectrum appear after the addition of BTMA to the sample compartment, of which the lowest energy transition at 35,964 cm^{-1} marked 'C' is the band origin transition of phenol–BTMA. This transition is red shifted by 384 cm^{-1} from the corresponding band of bare phenol, and the shift is larger than that of phenol–H_2O (355 cm^{-1}) and smaller than that of phenol–MeOH (415 cm^{-1}). Fig. 7(b) shows the FDIR spectrum of phenol–BTMA, which was recorded by probing the cluster band 'C' in Fig. 7(a). A single broad transition at 3514 cm^{-1} corresponds to the O–H stretching vibration of the cluster. It is well documented in literature that the O–H stretching of bare phenol occurs at 3657 cm^{-1} [8,43]. This implies that the O–H stretching vibration of phenol shifts to a lower frequency by 143 cm^{-1} upon the complexation with BTMA, which is larger than in the case of phenol–H_2O (133 cm^{-1}) and smaller than that of phenol–MeOH (201 cm^{-1}). The spectral shifts, both in electronic as well as vibrational transitions are well correlated with each other, and indicate that phenol acts as a proton donor to BTMA, similar to that in phenol–H_2O and phenol–MeOH clusters. This unequivocally establishes the formation of hydrogen bonding between phenolic O–H and BTMA.

The LIF excitation spectrum of phenol in the presence of BTMA shows several new transitions. In order to determine the origin of these transitions, i.e., to examine the possibility of isomers and other species, IR–UV hole-burning spectroscopy was carried out. Trace I of Fig. 7(c) is the LIF excitation spectrum, which is identical to Fig. 7(a), and trace II is the IR–UV hole-burnt spectrum, which was recorded by pumping the O–H stretching vibration of phenol–BTMA at 3514 cm^{-1} with an IR laser prior to the UV excitation. It is evident that all the transitions, except the peak marked 'W,' appearing in the LIF excitation spectrum (trace I) have diminished intensities in the hole-burn spectrum (trace II). This establishes the presence of only one isomer of phenol–BTMA. Trace III is the LIF excitation spectrum of phenol–BTMA obtained by subtracting II from I, which shows rich vibronic activity.

4.1.2. Phenol–BDMA

Fig. 8(a) shows the LIF excitation spectrum of phenol–borane-dimethylamine (BDMA). The transition marked 'C' at 39,249 cm^{-1} is the band origin transition of phenol–BDMA, which is red shifted from the corresponding transition of bare phenol by 89 cm^{-1}. Accompanying the band origin transition are the low frequency vibronic bands, marked with asterisk, corresponding to intermolecular modes. Fig. 8(b) shows the FDIR spectrum of phenol–BDMA, in which the peak at 3272 cm^{-1} was assigned to the N–H stretching of the BDMA moiety, based on the energy considerations. Since the gas phase IR spectrum of bare BDMA in not known, it was not possible to compare it with N–H stretching of bare BDMA. Further, an intense transition at 3483 cm^{-1} was

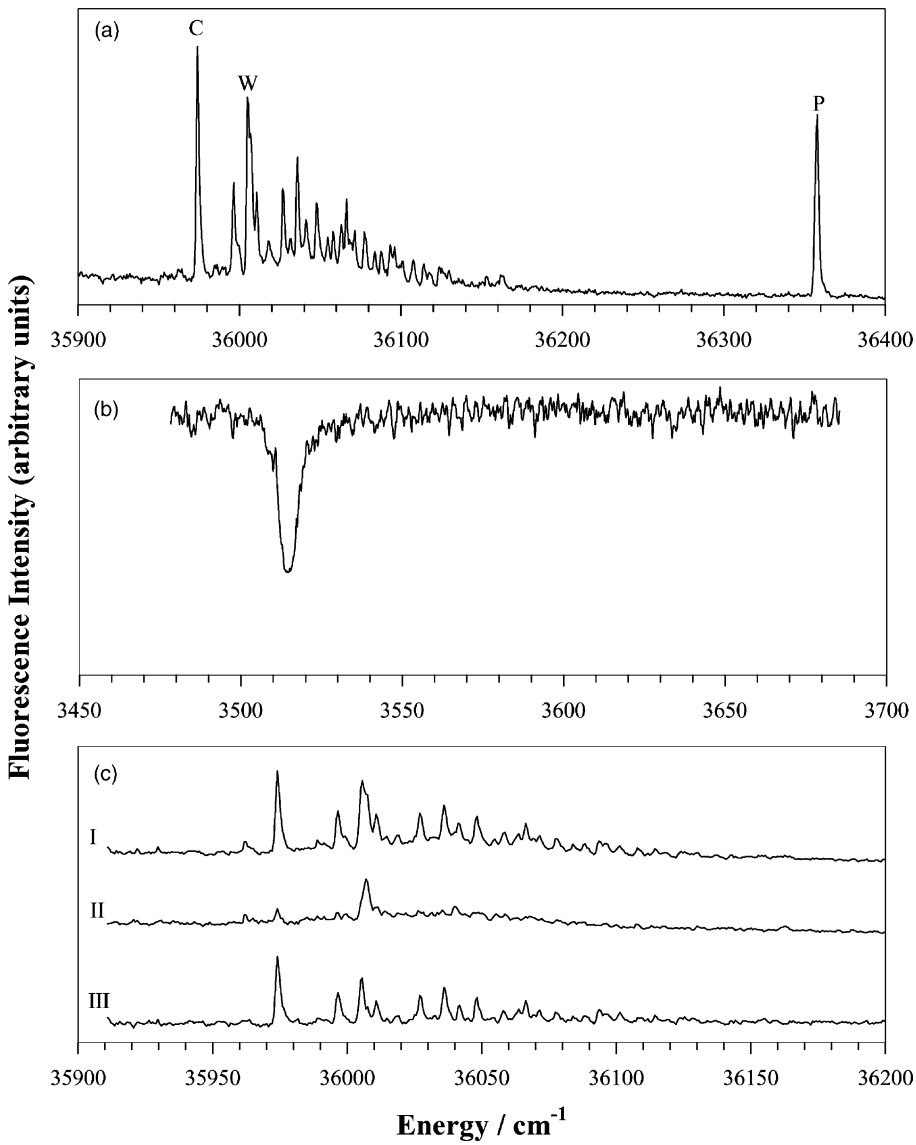

Fig. 7. (a) LIF excitation spectrum of phenol in the presence of BTMA. The peaks marked C, W, and P are the origin bands of phenol–BTMA, phenol–H_2O, and bare phenol, respectively. (b) FDIR spectrum of phenol–BTMA. (c) LIF excitation spectrum with IR off (I), IR–UV hole-burnt spectrum (II), and LIF excitation spectrum of phenol–BTMA (III = II − I).

assigned to the phenolic O–H stretching in the cluster, which is shifted by 174 cm^{-1} to a lower frequency from that of bare phenol. This shift is comparable to many other hydrogen bonded clusters of phenol, and suggests that phenolic O–H is undoubtedly hydrogen bonded to BDMA. Furthermore, four bands were observed on the high frequency side of the O–H stretching vibration with excess energies of 19, 31, 44, and 47 cm^{-1}. These bands were assigned to combinations of intermolecular vibrations on the O–H stretching vibration. Similar combination bands accompanied by hydrogen bonded O–H/N–H stretching vibration

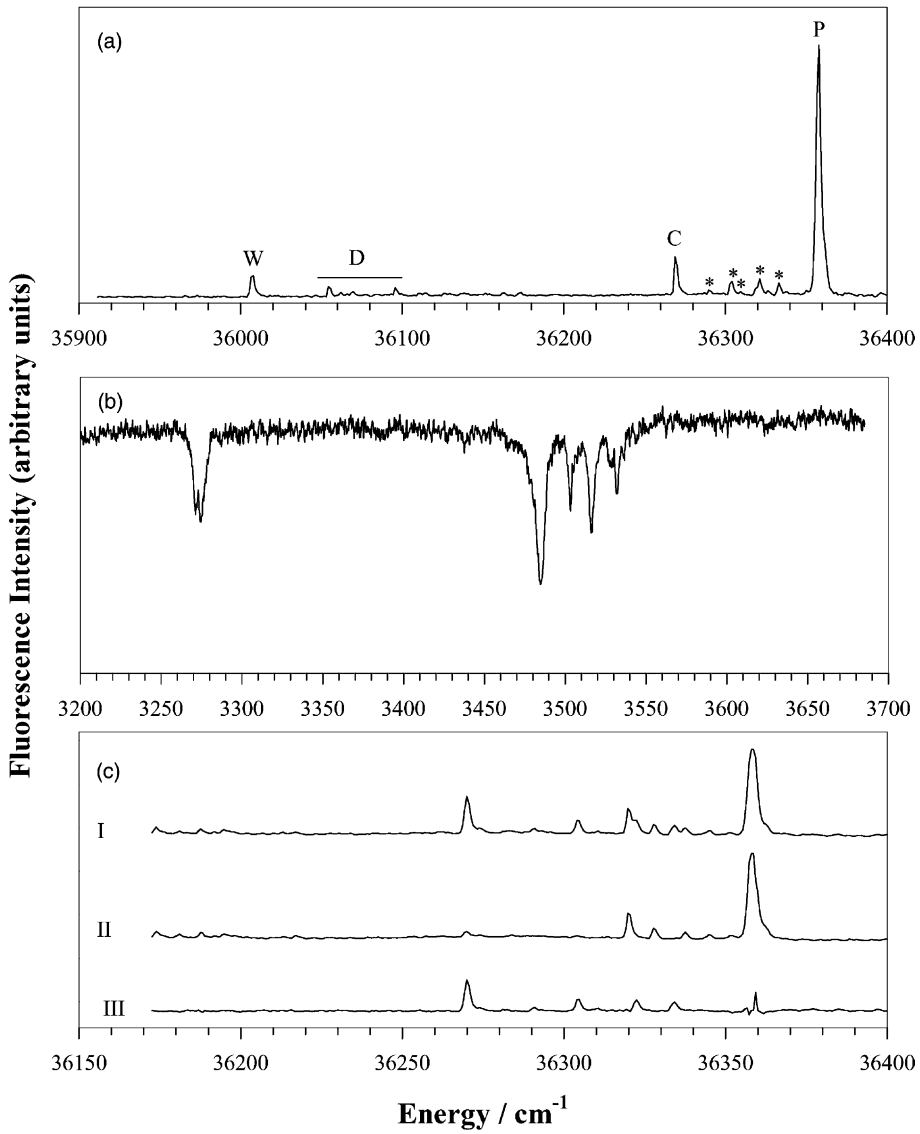

Fig. 8. (a) LIF excitation spectrum of phenol in the presence of BDMA. The transition marked 'C' is the band origin of phenol–BDMA complex and those marked with asterisk are the accompanying vibronic bands. The bands marked P, W, and D are due to bare phenol, phenol–H_2O, and phenol dimer, respectively. (b) FDIR spectrum of phenol–BDMA, and (c) LIF excitation spectrum with IR off (I), IR–UV hole-burnt spectrum (II), and LIF excitation spectrum of phenol–BDMA (III = II − I).

have been observed in several cases [79,80], which indicates a strong intermolecular interaction.

Despite the small red shift of 89 cm^{-1} in the electronic transition, a large shift of 174 cm^{-1} in the O–H stretching to a lower frequency confirms that phenol is hydrogen bonded to BDMA. The shifts in the electronic and O–H vibrational transitions do not correlate with each other as well as in the case of phenol–BTMA. A survey of various hydrogen bonded phenol clusters points towards the fact that the

electronic transition shifts to the red when phenol is a proton donor, while it shifts to the blue if phenol is a proton acceptor. On the other hand, only clusters in which phenol acts as a proton donor show a substantial low frequency shift of the O–H stretching. In the case of phenol–$(H_2O)_2$, which has a cyclic structure with phenol acting as both a proton donor and an acceptor, the red shift in the electronic transition is only 133 cm^{-1} while the O–H stretching frequency shows a substantial shift of 269 cm^{-1} to a lower frequency [81]. This trend is very similar to that observed in the present case. Extending the analogy it is reasonable to assume that phenol–BDMA forms a cyclic structure. Also, here we rule out the cyclic complex with N–H of BDMA moiety hydrogen bonded with π-cloud of phenyl ring, because, in that event the shift in the electronic transition would be much larger to the red than observed in the present case. This is due to fact that both π-electron bound clusters and proton donating clusters of show red shift in the electronic transition.

Even in the case of phenol–BDMA, several new transitions appeared in the LIF excitation spectrum whose origin was determined by IR–UV hole-burning spectroscopy. Traces I and II in Fig. 8(c) are the LIF excitation spectrum and IR–UV hole-burnt spectrum, respectively, and trace III is the LIF excitation spectrum of phenol–BDMA, which was obtained by subtraction of trace II from trace I. This also shows the presence of only one species phenol–BDMA, and exhibits a rich vibronic activity. Couple of extra peaks, which can be seen in traces I and II are not due to phenol–BDMA, as confirmed by mass resolved excitation spectrum [29].

4.1.3. 2PY–BTMA

Fig. 9(a) shows the LIF excitation spectrum of 2PY in the presence of BTMA; peaks A at 29,831 and B at 29,928 cm^{-1} are band origins of bare 2PY corresponding to two different N–H conformations in S_1 [82]. Of numerous transitions that can be seen in the excitation spectrum, the transition at 30,034 cm^{-1}, marked with 'C,' is the origin band of 2PY–BTMA, which was assigned on the basis of IR–UV hole-burning spectroscopy. The origin band of 2PY–BTMA is shifted to the blue by 203 cm^{-1} from the corresponding band marked by 'A' of bare 2PY. Once again several vibronic transitions accompanied with the band origin are associated with low frequency vibrational motions of the cluster. Transitions marked with 'R' in the excitation spectrum are thought to be due to some reaction products between 2PY and BTMA.

The extent of the blue shift in the present case is marginally larger than the 2PY cluster with dioxane (120 cm^{-1}) and with dimethylether (131 cm^{-1}), but much smaller than in the cases of 2PY–H_2O (633 cm^{-1}), 2PY–MeOH (615 cm^{-1}), and 2PY dimer (944 cm^{-1}) [79]. The electronic transition of 2PY clusters shifts much further to the blue if the solvent molecule interacts with both the N–H and carbonyl groups forming a cyclic structure, as in the case of clusters with H_2O, MeOH and in the dimer. This is due to the interaction of the solvent proton with the carbonyl oxygen of 2PY, which is destabilized upon electronic excitation. On the other hand, when the solvent interacts primarily with the N–H group the blue shift is much smaller, as in the cases of 2PY–dioxane and dimethylether. Therefore, the present blue shift in the electronic transition suggests that BTMA primarily interacts with the N–H site of 2PY.

Fig. 9(b) shows the FDIR spectrum of 2PY–BTMA in the ring C–H and the N–H stretching frequency region. The somewhat broad transition at 3293 cm^{-1} is the N–H stretching of the 2PY moiety in the cluster, which is shifted to a lower frequency by 155 cm^{-1} in comparison with bare 2PY (3448 cm^{-1}) [79]. This once again suggests that BTMA interacts with the N–H site of the 2PY moiety, which is in line with the observed electronic blue shift. The shifting of N–H stretching to a lower frequency in the present case is more than that of 2PY–H_2O (119 cm^{-1}) and 2PY–MeOH (121 cm^{-1}) and less than that of 2PY–dioxane (226 cm^{-1}) and 2PY–dimethylether (250 cm^{-1}) [79]. Furthermore, two low frequency intermolecular modes can also be seen in the FDIR spectrum, which appear in combination with the N–H stretching, and indicates the formation of a strong hydrogen bond between N–H group of 2PY and BTMA. As regards to the transitions marked with 'R' in the

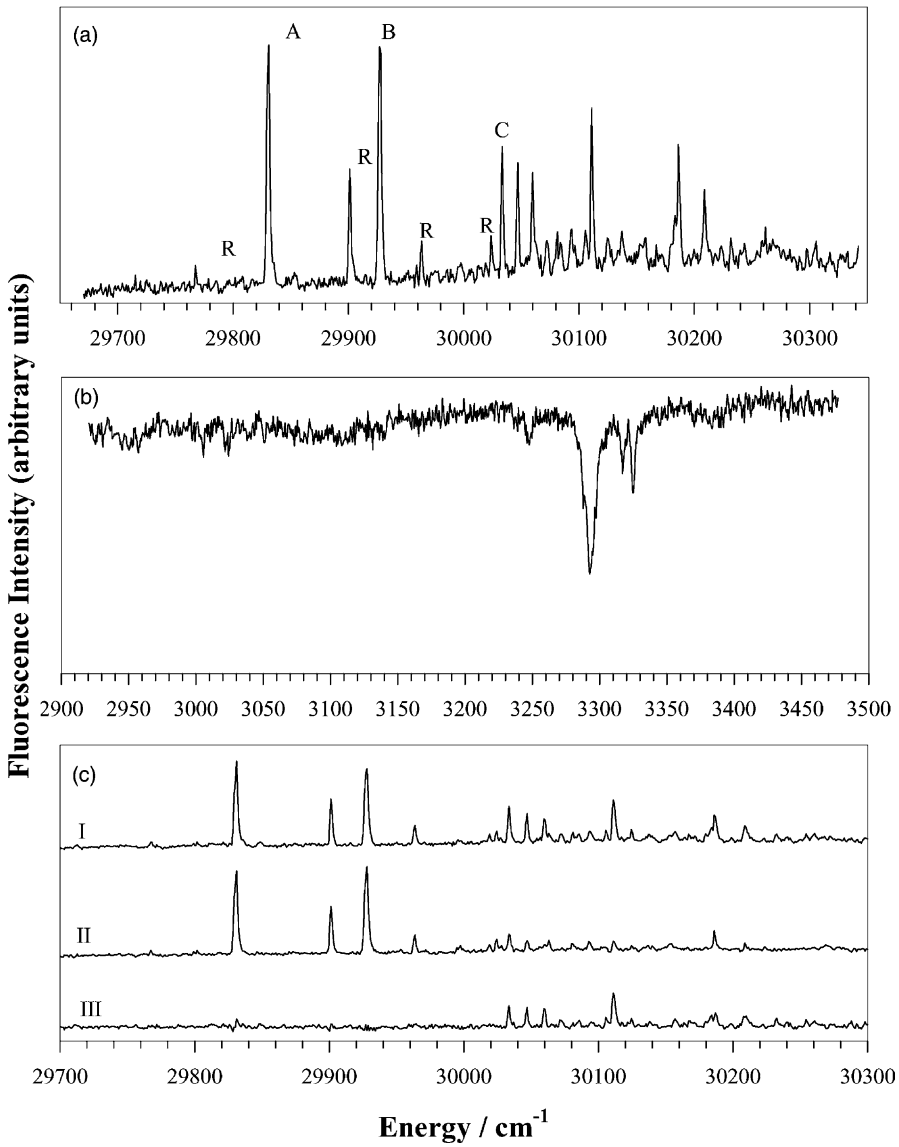

Fig. 9. (a) LIF excitation spectrum of 2PY in the presence of BTMA. Peaks marked A, B are the two band origins of the bare molecule, C is the cluster with BTMA, and Rs are some reaction product between 2-pyridone and BTMA. (b) FDIR spectrum of 2PY–BTMA. (c) LIF excitation spectrum with IR off (I), IR–UV hole-burnt spectrum (II), and LIF excitation spectrum of 2PY–BTMA (III = II − I).

LIF excitation spectrum (Fig. 9(a)), no IR band was observed in the FDIR spectrum corresponding to both N–H and C–H stretching vibrations [31]. On the other hand, the similar electronic transition energy as that of 2PY suggests that the 2PY chromophore is intact. The similarity of the electronic transition energy and the disappearance of N–H stretching indicates possibility of a reaction between 2PY and BTMA leading to some substitution on the pyridine ring, which did not alter the $S_1 \leftarrow S_0$ electronic excitation energy. Fig. 9(c) once again shows the IR–UV hole-burning spectrum along with the LIF excitation spectra,

which confirms the presence of only one isomer of 2PY–BTMA, similar to the two earlier cases.

4.1.4. Structures of the dihydrogen bonded clusters

The above-mentioned experimental results clearly indicate that phenolic O–H is hydrogen bonded to both BTMA and BDMA, and also the N–H site of 2PY is hydrogen bonded to BTMA. It is well known that in crystals of borane–amines the B–H σ-bond acts as a proton acceptor of acidic N–H group [24]. Extending the analogy it would be easy to deduce that the present clusters of phenol and 2PY are dihydrogen bonded. Moreover, in both BTMA and BDMA the B–H group is the only site accessible as a strong proton acceptor. In order to verify this, we carried out density functional theory (B3LYP) calculation using 6–31++G (d,p) basis set, since this level of theory has shown remarkable results for the dihydrogen bonded structures at a reasonable computational cost [83].

Fig. 10(a) shows the calculated structure of phenol–BTMA, which is the only minimum we found irrespective of the starting geometry for calculation. In this cluster the interaction between phenolic proton and hydrogen atoms attached to boron, forming a pair of bifurcated dihydrogen bonds, can be clearly seen. The ZPE and BSSE corrected stabilization energy is 4.44 kcal/mol. For the first dihydrogen bond the H···H contact distance is 1.87 Å, B–H···H angle is 103.0° and the O–H···H angle is 151.4°. The corresponding values for the second dihydrogen bond are 2.25 Å, 84.1°, and 143.0°, respectively. In the case of phenol–BDMA we found three minima in the PES, whose ZPE and BSSE corrected stabilization energies were 6.22, 4.37, and 3.74 kcal/mol. From the stabilization energies it can be concluded, straightforwardly, that only the most stable isomer will be significantly populated in the supersonic jets with the nozzle temperature of 310 K, and indeed, only one species of phenol–BDMA was observed. Fig. 10(b) shows the structure of the most stable form of phenol–BDMA, in which a six-member ring O–H–H–B–N–H–(O) is formed with phenol acting both as a proton donor and an acceptor. Once again phenolic O–H group interacts with hydrogen on boron forming a dihydrogen bond. In this case, the H···H contact distance is 1.87 Å, B–H···H angle is 100.0° and the O–H···H angle is 143.4°. Additionally, a conventional hydrogen bond is formed between the N–H site of the BDMA moiety and the phenolic oxygen. For this hydrogen bond, phenol acts a proton acceptor, with the hydrogen bond distance of 2.15 Å and N–H···H angle being 139.2°. This structure is very much in accordance with the predicted one on the basis of spectral shifts in the electronic and O–H stretching transitions. The second (local) minimum (figure not shown), which has stabilization energy of 4.37 kcal/mol, has an intermolecular structure almost identical to phenol–BTMA with the two H···H contact distances of 1.86, 2.30 Å, B–H···H angles are 100.0, 82.9° and the O–H···H angles being 150.1, 142.9°. The third is also a local minimum (figure not shown), whose stabilization energy is 3.74 kcal/mol was a conventional hydrogen bonded cluster with the phenol site being an acceptor with the hydrogen bonding distance of 2.07 Å and N–H···O angle of about 176.5°.

The structure of 2PY–BTMA is given in Fig. 10(c). Even in this case we found only one minimum on the PES irrespective of initial geometry. The ZPE and BSSE corrected stabilization energy of the cluster is 6.84 kcal/mol. In this cluster the N–H proton of 2PY forms a dihydrogen bond with hydrogen atom attached to boron of the BTMA moiety. In the dihydrogen bond the distance between the two hydrogens is 1.78 Å with the B–H···H angle of 117.5° and N–H···H angle is 139.3°. Furthermore, a weak hydrogen bond of length 2.29 Å between a methyl proton of the BTMA moiety and the carbonyl oxygen of 2PY gives an additional stability. This weak interaction of methyl protons with the carbonyl oxygen gives the 2PY–BTMA cluster a marginally larger blue shift in comparison with the case of the clusters of dioxane and dimethylether.

In all three cases the short H···H distance (less than 2.0 Å), the strongly bent B–H···H angles and the nearly linear O/N–H···H angles indicate the formation of dihydrogen bonds and are very much in accordance with the geometrical parameters observed in crystals of borane–amines. The comparison and agreement between the calculated and observed

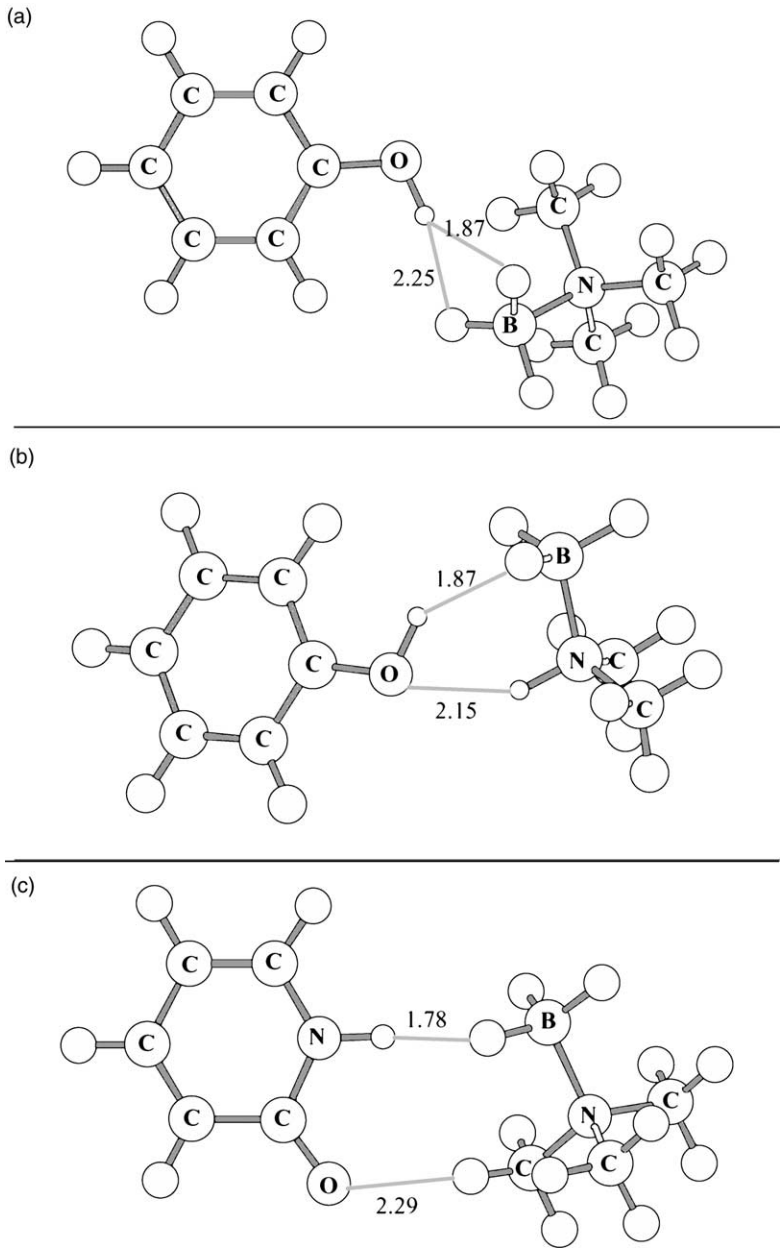

Fig. 10. Energy optimized structures of (a) phenol–BTMA, (b) phenol–BDMA, and (c) 2PY–BTMA clusters.

vibrational frequencies serves as a benchmark for the structural assignment of the clusters. In Fig. 11 the FDIR spectra of phenol–BTMA, phenol–BDMA, and 2PY–BTMA are shown along with the calculated vibrational frequencies for the respective structures, which are given in Fig. 10. The agreement between the experimental and calculated values is clearly evident in all the three cases. In the case of phenol–BTMA (Fig. 11(a)) the observed and calculated values of O–H stretching vibration are 3514 and 3504 cm^{-1},

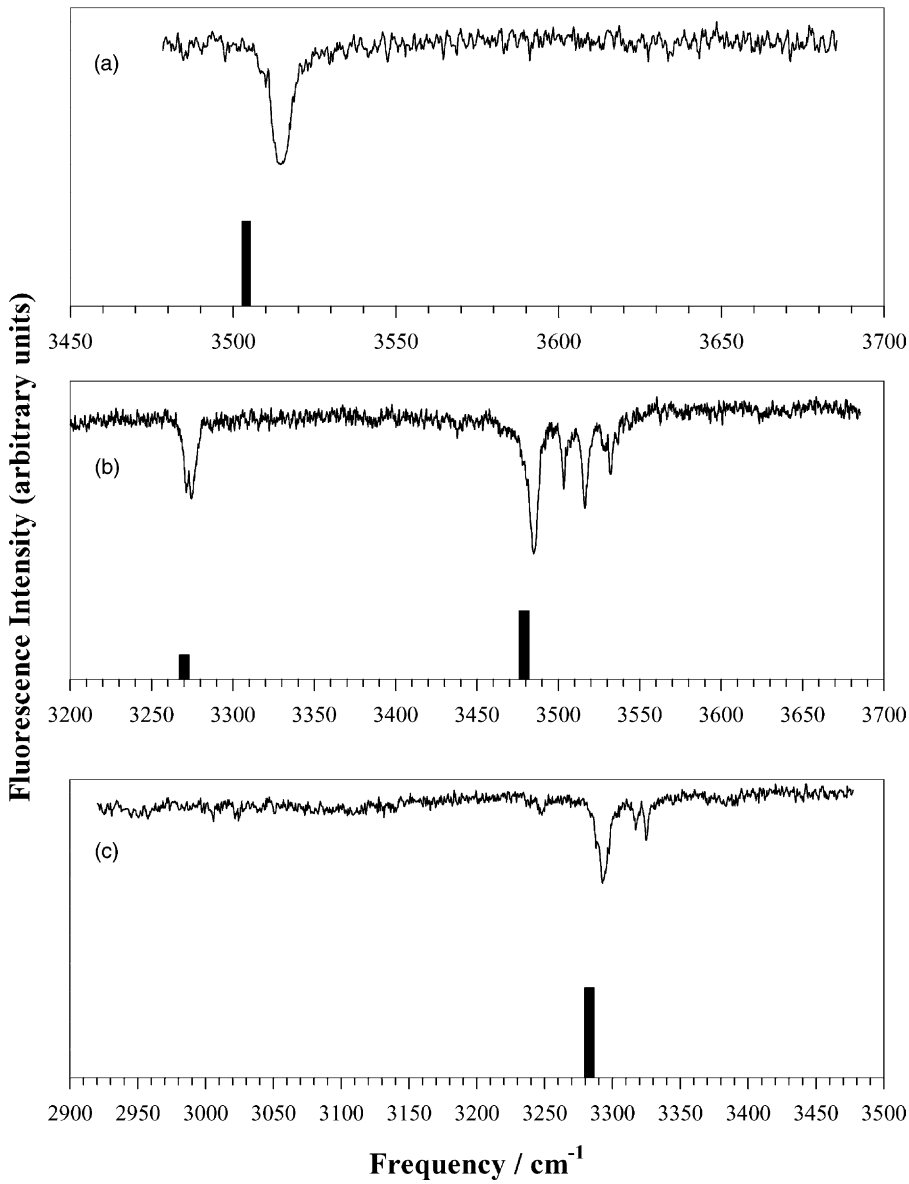

Fig. 11. Comparison of experimental and calculated IR spectra of (a) phenol–BTMA, (b) phenol–BDMA, and (c) 2PY–BTMA clusters.

respectively. For phenol–BDMA (Fig. 11(b)) the experimental frequencies for the N–H and O–H stretching vibrations are 3272 and 3483 cm^{-1}, respectively, while the corresponding calculated values are 3270 and 3479 cm^{-1}, respectively. Finally, in the case of 2PY–BTMA (Fig. 11(c)) the N–H stretching occurs at 3293 cm^{-1}, while the calculated value is 3282 cm^{-1}. In all the three clusters, the agreement between the experimental N–H/O–H stretching frequencies and the calculated values is excellent (less than 3% deviation) and the corresponding structures can be considered as the most probable structures for phenol–BTMA,

phenol–BDMA and 2PY–BTMA. The experimental results together with the calculated results unequivocally establish the formation of B–H···H–X (X = O, N) dihydrogen bonded clusters in the gas phase.

4.2. Dehydrogenation reaction

While performing one color $S_1 \leftarrow S_0$ REMPI of phenol–BTMA, extensive fragmentation was observed even under a mild focusing condition of the laser. Fig. 12(a) shows a low-resolution mass spectrum following REMPI, in which the parent ion signal occurs at 167 amu, intense peaks at 58 and 70 amu, and weak peaks at 77 and 90 amu. Surprisingly, the signal corresponding to phenol ion at 94 amu was extremely weak. This spectrum was recorded by saturating the strongest signal at 58 amu so that very weak signals can be observed. Since the detection time of the quadrupole mass filter used in this experiment is about few tens of microseconds after the ionization, the fragmentation is complete and the relative abundance of various mass fragments reflects their stability. A high-resolution mass spectrum is reproduced in Fig. 12(b) showing mass peaks at 72, 70, 58, and 56 amu, which are the intense signals in the low-resolution mass spectrum. The intensity differences observed in the two spectra is due to the saturation of signal at 58 amu in Fig. 12(a). Also seen in the high-resolution mass spectrum are signals at 71 and 69 amu, which are about 20% in intensity with respect to signals at 72 and 70 amu, respectively, which implies the presence of boron in these mass fragments since the isotopes 11 and 10 of boron are in the ratio 8:2. Fig. 13 shows the mass resolved excitation spectra,

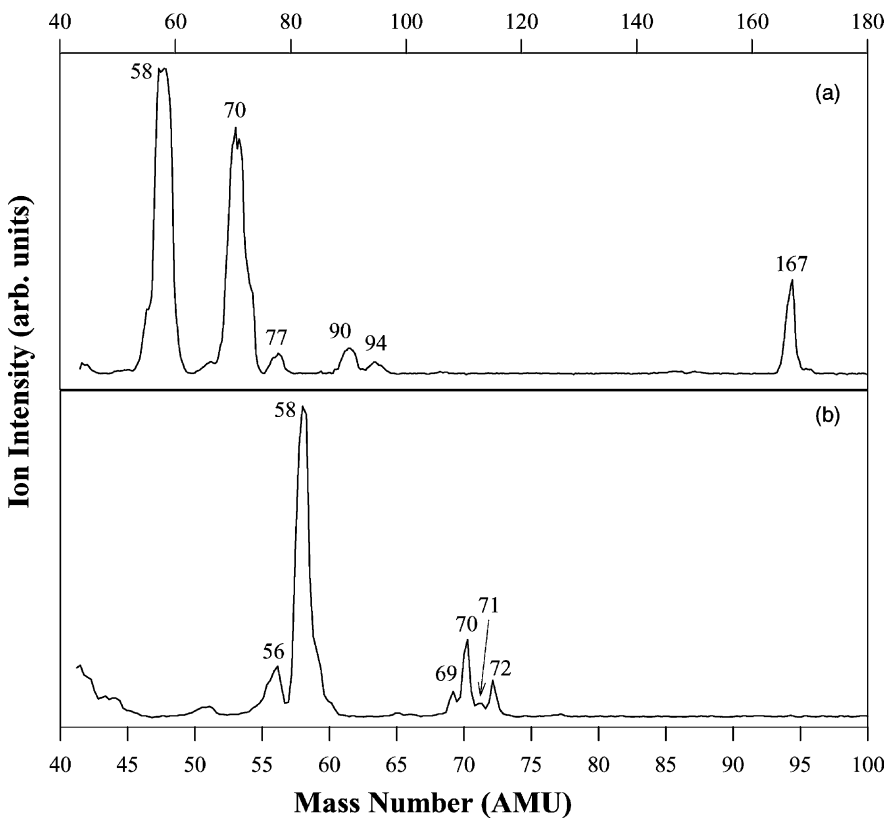

Fig. 12. (a) Low-resolution mass spectrum of phenol–BTMA cluster upon photoionization and (b) high-resolution mass spectrum.

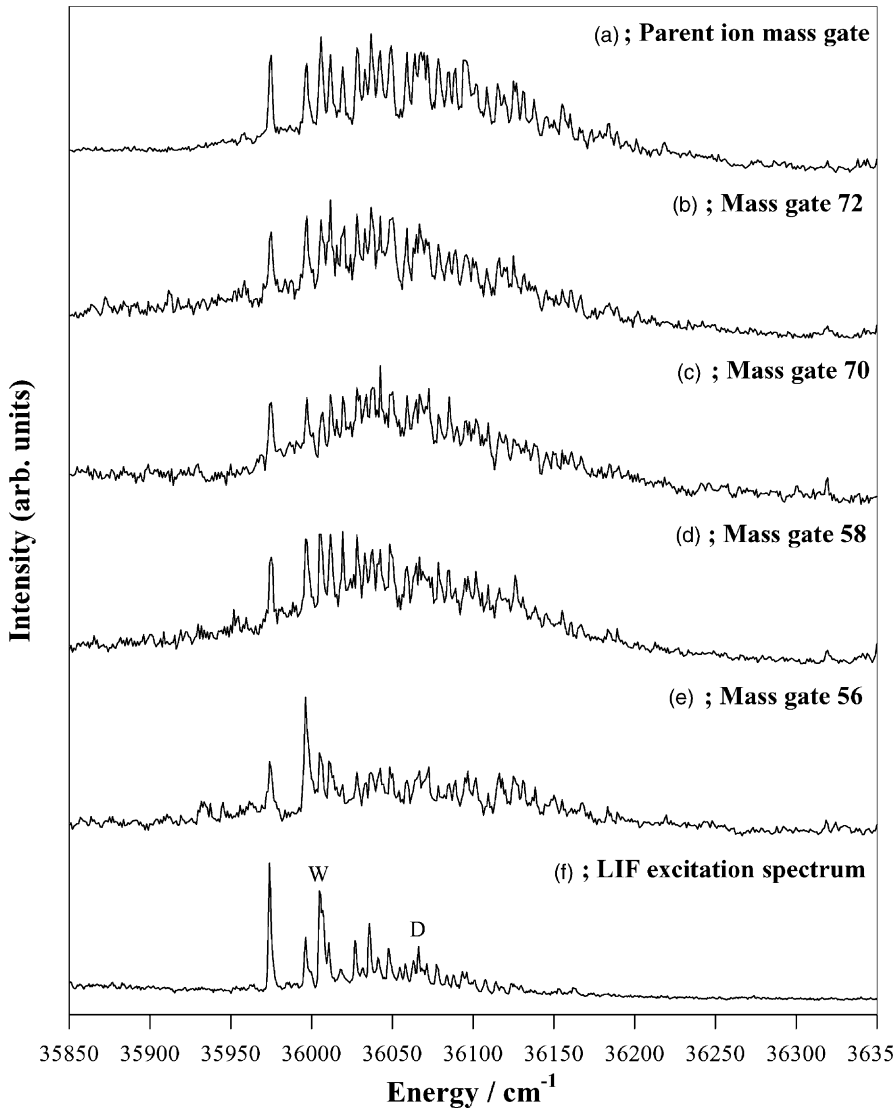

Fig. 13. (a–e) Mass resolved $S_1 \leftarrow S_0$ excitation (action) spectra following REMPI of phenol–BTMA cluster with mass gates at 167, 72, 70, 58, and 56 amu, respectively, and (f) is the LIF excitation spectrum. Peaks marked W and D in the LIF excitation spectrum are due to phenol–H_2O and phenol dimer, respectively.

which were recorded by gating various observed mass signals, along with the LIF excitation spectrum. Good agreement between all the spectra within the experimental uncertainties establishes the origin of all the mass fragments as the parent phenol–BTMA cluster ion.

The fragmentation of hydrogen bonded clusters of phenol following ionization with moderate to intense lasers produces phenol cation in many cases. The known exceptions to this are the phenol clusters of trialkylamines, such as phenol–trimethylamine, wherein the proton is transferred from phenol to

trimethylamine following ionization [84]. In this case the mass spectrum shows a relatively low intensity of the parent cluster ion and an intense protonated trimethylamine $[HNCH_3)_3{}^+]$, and no signal corresponding to phenol cation. The absence (or very small amount) of phenol cation upon photoionization of phenol–BTMA has the striking similarity with the mass spectral characteristics observed in the case of phenol–trimethylamine, suggesting the loss of proton from phenol moiety in the cluster cation.

To explain the observed mass spectral pattern we propose the following photo-fragmentation scheme, which is shown in Fig. 14. In this scheme, the phenol–BTMA cation **1** (schematic representation), absorbs an additional photon upon ionization generating a large internal energy in the cation, which leads to subsequent fragmentation. As mentioned earlier, the

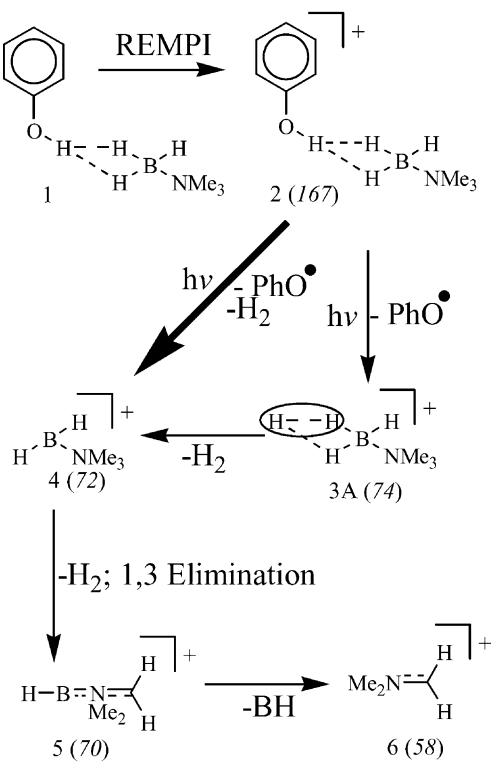

Fig. 14. Scheme depicting the photo-fragmentation of phenol–BTMA cluster cation. The italicized numbers in parenthesis are the mass numbers of the corresponding fragment.

absence of phenol cation following the fragmentation suggests a possibility of intracluster proton transfer from phenol to BTMA. This would therefore lead to the 74 mass fragment, **3**, which, however, was not observed. On the other hand, we observe the 72 mass fragment **4**, which is one mass unit less than BTMA. Subsequent fragmentation leading to mass fragments 70 (**5**), 58 (**6**), and 56 amu can be rationalized, as illustrated in the photo-fragmentation scheme. In the present case the absence of the 74 mass signal might be due to the large internal energy in the phenol–BTMA cation. However, even a two-color REMPI that would deposit less amount of internal energy in the system gave an identical fragmentation pattern.

In the case of hydrogen bonded phenol clusters the intracluster proton transfer reaction $C_6H_5OH^+\cdots X \rightarrow C_6H_5O\cdots HX^+$ would be feasible only if the proton affinity of X is about 205 kcal/mol or greater [85]. The spectral shifts in both the electronic and O–H stretching transitions for hydrogen bonded clusters of phenol are correlated linearly with the proton affinity of the solvent molecules. In the case of phenol–BTMA, the spectral shift in both the electronic and O–H stretching transitions are larger than that of phenol–H_2O and smaller than that of phenol–MeOH [45]. Therefore, from the spectral shifts the proton affinity of the dihydrogen bonding site of BTMA should lie between 165 kcal/mol (H_2O) and 180 kcal/mol (MeOH) [86] and can be estimated as 168 kcal/mol, which is much less than that required for intracluster proton transfer reaction. This justifies the absence of signal at 74. Further, it can be seen from the mass spectrum that apart from phenol moiety BTMA also loses a hydrogen atom. Therefore, it is reasonable to assume a three-body dissociation process of the phenol–BTMA cation leading to an elimination of phenoxy radical and molecular hydrogen as depicted by a bold arrow in Fig. 14.

An alternative scheme can also be considered to explain the observed mass spectral pattern based on the C–O bond fission [27], which is the origin of weak signals at 77 and 90 amu. However, this channel is considered to be minor since it originates from breaking of a C–O bond, which is not the weakest

bond in the molecule. Therefore, the fragmentation of the phenol–BTMA cation follows the elimination two interacting hydrogen atoms in the dihydrogen bond as molecular hydrogen leading to dehydrogenation reaction.

5. Concluding remarks

The experimental evidence, especially from the IR spectra, has unequivocally established the existence of unconventional hydrogen bonding. In the first case we found a large change either in the interaction energy or the structure upon ionization of π-hydrogen bonded clusters as exemplified in cases of phenol–benzene and benzene–water complexes, respectively. Further, in the cases of the methylphenol (cresol) and the ethylphenol cations, the small but definite shift in the O–H stretching vibration to a lower frequency occurs only in the case of *o–cis*-isomer cations, while no change is seen for all the rest of the rotational/structural isomers. The close proximity of alkyl group to the hydroxyl group in the *o–cis*-isomer and the lowering of O–H stretching frequencies represent that an unconventional O–H···C hydrogen bond is formed in the cationic state, for the methyl/alkyl group being a proton acceptor. In spite of seriously underestimating the shift in the O–H stretching vibration of *o–cis*-isomer, recent theoretical reports have given negative conclusions for the formation of unconventional hydrogen bonding. We believe that much higher-level calculations are required to catch the phenomenon and any conclusion regarding the presence/absence of unconventional O–H···C hydrogen bond in these systems should be based on the correct reproduction of observed vibrational frequencies.

In the case of phenol and 2PY clusters with borane–amine, the shifting of hydride stretching vibrations to lower frequencies establish their proton donating abilities in the binary clusters. Together with the DFT calculations the formation of the dihydrogen bond in these clusters was established. For the comprehensive understanding of dihydrogen bonding, the investigation of B–H stretching vibrations in borane–amines is very essential. Unfortunately, the current IR source in our laboratory does not cover the B–H stretching frequency region of 2300–2400 cm^{-1}. Efforts are being made in this direction and hopefully we will be able to investigate B–H stretching in the near future. As regards to the dehydrogenation reaction from the phenol–BTMA cation, the investigation of the cation cluster structure is the immediate goal.

References

[1] G.E. Pimentel, A.L. McClellan, The Hydrogen Bond, W.H. Freeman and Company, San Francisco, 1960.
[2] G.A. Jeffrey, An Introduction to Hydrogen Bonding, Oxford University Press, New York, 1997.
[3] S. Scheiner, Hydrogen Bonding, Oxford University Press, New York, 1997.
[4] E.R. Bernstein (Ed.), Atomic and Molecular Clusters, Elsevier, Amsterdam, 1990.
[5] M. Ito, J. Mol. Struct. 177 (1988) 173.
[6] R.H. Page, Y.R. Shen, Y.T. Lee, J. Chem. Phys. 88 (1988) 4621.
[7] C. Riehn, C. Lahmann, B. Wassermann, B. Brutschy, Chem. Phys. Lett. 197 (1992) 443.
[8] S. Tanabe, T. Ebata, M. Fujii, N. Mikami, Chem. Phys. Lett. 215 (1993) 347.
[9] R.N. Pribble, T.S. Zwier, Science 265 (1994) 75.
[10] T.S. Zwier, Ann. Rev. Phys. Chem. 47 (1996) 205.
[11] T. Ebata, A. Fujii, N. Mikami, Int. Rev. Phys. Chem. 17 (1998) 331.
[12] B. Brutschy, Chem. Rev. 100 (2000) 3891.
[13] M. Nishio, M. Hirota, Y. Umezawa, CH/π-Interaction: Evidence, Nature, and Consequences, Wiley, New York, 1998.
[14] H.-D. Barth, K. Buchhold, S. Djafari, R. Reimann, U. Lommatzsch, B. Brutschy, Chem. Phys. 239 (1998) 49.
[15] G.R. Desiraju, Acc. Chem. Res. 29 (1996) 441.
[16] A. Allerhand, P.R. von Schleyer, J. Am. Chem. Soc. 85 (1963) 1715.
[17] M.C. Rovira, J.J. Novoa, M.H. Whangbo, J.M. Williams, Chem. Phys. 200 (1995) 319.
[18] Y. Gu, T. Kar, S. Scheiner, J. Am. Chem. Soc. 121 (1999) 9411.
[19] M. Hartmann, S.D. Wetmore, L. Radom, J. Phys. Chem. A 105 (2001) 4470.
[20] A. Fujii, E. Fujimaki, T. Ebata, N. Mikami, J. Am. Chem. Soc. 120 (1998) 13256.
[21] E. Fujimaki, A. Fujii, T. Ebata, N. Mikami, J. Chem. Phys. 112 (2000) 137.
[22] A. Fujii, A. Iwasaki, K. Yoshida, T. Ebata, N. Mikami, J. Phys. Chem. A101 (1997) 1798.
[23] M. Miyazaki, A. Fujii, T. Ebata, N. Mikami, Chem. Phys. Lett. 349 (2001) 431.
[24] R.H. Crabtree, P.E.M. Siegbahn, O. Eisenstein, A.L. Rheingold, T. Koetzle, Acc. Chem. Res. 29 (1996) 348.

[25] A.J. Lough, S. Park, R. Ramachandran, R.H. Morris, J. Am. Chem. Soc. 116 (1994) 8356.
[26] T.B. Richardson, S. deGala, R.H. Crabtree, P.E.M. Sieghbahn, J. Am. Chem. Soc. 117 (1995) 12875.
[27] G.N. Patwari, T. Ebata, N. Mikami, J. Phys. Chem. A 105 (2001) 10753.
[28] J.L. Atwood, G.A. Koutsantonis, F. Lee, C.L. Raston, J. Chem. Soc., Chem. Commun. (1994) 91.
[29] G.N. Patwari, T. Ebata, N. Mikami, J. Chem. Phys. 113 (2000) 9885.
[30] G.N. Patwari, T. Ebata, N. Mikami, J. Chem. Phys. 114 (2001) 8877.
[31] G.N. Patwari, T. Ebata, N. Mikami, J. Phys. Chem. A 105 (2001) 8462.
[32] A. Mitsuzuka, A. Fujii, T. Ebata, N. Mikami, J. Chem. Phys. 105 (1996) 2618.
[33] R.J. Lipert, S.D. Colson, Chem. Phys. Lett. 161 (1989) 303.
[34] L.I. Yeh, M. Okumura, J.D. Nyers, J.M. Price, Y.T. Lee, J. Chem. Phys. 91 (1989) 7319.
[35] T. Sawamura, A. Fujii, S. Sato, T. Ebata, N. Mikami, J. Phys. Chem. 100 (1996) 8131.
[36] C.J. Weinheimer, J.M. Lisy, J. Chem. Phys. 105 (1996) 2938.
[37] T. Nakanaga, K. Kawamata, F. Ito, Chem. Phys. Lett. 279 (1997) 309.
[38] C. Unterberg, A. Jansen, M. Gerhards, J. Chem. Phys. 113 (2000) 7945.
[39] A. Fujii, A. Iwasaki, T. Ebata, N. Mikami, J. Phys. Chem. A101 (1997) 5963.
[40] E. Fujimaki, A. Fujii, T. Ebata, N. Mikami, J. Chem. Phys. 110 (1999) 4238.
[41] M. Gerhards, M. Schiwek, C. Unterberg, K. Kleinermanns, Chem. Phys. Lett. 297 (1998) 515.
[42] N. Mikami, A. Okabe, I. Suzuki, J. Phys. Chem. 92 (1988) 1858.
[43] H.D. Bist, J.C.D. Brand, D.R. Williams, J. Mol. Spectrosc. 24 (1967) 413.
[44] G.V. Hartland, B.F. Henson, V.A. Venturo, P.M. Felker, J. Phys. Chem. 96 (1992) 1164.
[45] A. Iwasaki, A. Fujii, T. Ebata, N. Mikami, J. Phys. Chem. 100 (1996) 16053.
[46] Y. Inokuchi, N. Nishi, Ann. Rev. Inst. Mol. Sci. (1999) 66.
[47] O. Dopfer, K. Müller-Dethlefs, J. Chem. Phys. 101 (1994) 8508.
[48] I. Fischer, R. Linder, K. Müller-Dethlefs, J. Chem. Soc., Faraday Trans. 90 (1994) 2425.
[49] A. Fujii, T. Ebata, N. Mikami, J. Phys. Chem. A, in press.
[50] P. Ayotte, G.H. Weddle, J. Kim, M.A. Johnson, J. Am. Chem. Soc. 120 (1998) 12361.
[51] K. Ohashi, H. Izutsu, Y. Inokuchi, K. Hino, N. Nishi, H. Sekiya, Chem. Phys. Lett. 321 (2000) 406.
[52] K. Ohashi, Y. Nakae, Y. Inokuchi, Y. Nakai, N. Nishi, Chem. Phys. Lett. 239 (1998) 429.
[53] K. Ohashi, N. Nishi, J. Phys. Chem. 96 (1992) 2931.
[54] J.L. Knee, L.R. Khunder, A.H. Zweil, J. Chem. Phys. 87 (1987) 115.
[55] D.R. Lide (Ed.), CRC Handbook of Chemistry and Physics, 76th Edition, CRC Press, Boca Raton, FL, 1995.
[56] T. Bürgi, T. Droz, S. Leutwyler, Chem. Phys. Lett. 246 (1995) 291.
[57] S. Suzuki, P.G. Green, R.E. Bumgarner, S. Dasgupte, W.A. Goddard III, G.A. Blake, Science, 1992, p. 942.
[58] R.N. Pribble, T.S. Zwier, Faraday Dis. 97 (1994) 1.
[59] R.N. Pribble, A.W. Garret, K. Haber, T.S. Zwier, J. Chem. Phys. 103 (1995) 531.
[60] B.-M. Cheng, J.R. Grover, E.A. Walters, Chem. Phys. Lett. 232 (1995) 364.
[61] S.Y. Fredericks, K.D. Johdan, T.S. Zwier, J. Phys. Chem. 100 (1996) 7810.
[62] D. Feller, J. Phys. Chem. A103 (1999) 7558.
[63] P. Tarakeshwar, H.S. Choi, S.J. Lee, J.Y. Lee, K.S. Kim, T.-H. Ha, J.H. Jang, J.G. Lee, H. Lee, J. Chem. Phys. 111 (1999) 5838.
[64] W. Kim, D. Neuhauser, M.R. Wall, P.M. Felker, J. Chem. Phys. 110 (1999) 8461.
[65] A. Courty, M. Mons, I. Dimicoli, F. Piuzzi, M.-P. Gaigeot, V. Brenner, P. de Pujo, P. Millie, J. Phys. Chem. A102 (1998) 6590.
[66] H. Tachikawa, M. Igarashi, J. Phys. Chem. A102 (1998) 8648.
[67] H. Tachikawa, M. Igarashi, T. Ishibashi, Phys. Chem. Chem. Phys. 3 (2001) 3052.
[68] N. Solcà, O. Dopfer, Chem. Phys. Lett. 347 (2001) 59.
[69] A. Fujii, E. Fujimaki, T. Ebata, N. Mikami, J. Chem. Phys. 112 (2000) 6275.
[70] S.R. Langhoff, J. Phys. Chem. 100 (1996) 2819.
[71] A. Oikawa, H. Abe, N. Mikami, M. Ito, J. Phys. Chem. 88 (1984) 5180.
[72] A. Oikawa, H. Abe, N. Mikami, M. Ito, Chem. Phys. Lett. 116 (1985) 50.
[73] T. Aota, T. Ebata, M. Ito, J. Phys. Chem. 93 (1983) 3519.
[74] H. Mizuno, K. Okuyama, T. Ebata, M. Ito, J. Phys. Chem. 91 (1987) 5589.
[75] M.M. Szczesniak, G. Chalasinski, S.M. Cybulski, P. Cieplak, J. Chem. Phys. 98 (1993) 3078.
[76] C. Trindle, J. Phys. Chem. A104 (2000) 5298.
[77] J.C. Vank, S.J.K. Jensen, T.-H. Tang, I.G. Csizmadia, J. Mol. Struct. (Theochem.) 537 (2001) 189.
[78] D.W. Boo, Y.T. Lee, J. Chem. Phys. 103 (1995) 520.
[79] Y. Matsuda, T. Ebata, N. Mikami, J. Chem. Phys. 110 (1999) 8397.
[80] G.M. Florio, C.J. Gruenloh, R.C. Quimpo, T.S. Zwier, J. Chem. Phys. 113 (2000) 1143.
[81] T. Watanabe, T. Ebata, S. Tanabe, N. Mikami, J. Chem. Phys. 105 (1996) 408.
[82] M.R. Nimlos, D.F. Kelley, E.R. Bernstein, J. Phys. Chem. 93 (1989) 643.
[83] S.A. Kulkarni, J. Phys. Chem. A 102 (1998) 7704.
[84] N. Mikami, I. Suzuki, A. Okabe, J. Phys. Chem. 91 (1987) 5242.
[85] S. Sato, N. Mikami, J. Phys. Chem. 100 (1996) 4765.
[86] E.P.L. Hunter, S.G. Lias, J. Phys. Chem. Ref. Data 27 (1998) 413.